Journal of Hazardous Materials 175 (2010) 258–266

Contents lists available at ScienceDirect

Journal of Hazardous Materials

journal homepage: www.elsevier.com/locate/jhazmat

Enhanced photocatalytic activity for titanium dioxide by co-modifying with silica and fluorine

Shaogui Yang[a,*], Cheng Sun[a,*], Xinyong Li[b], Zhongqiang Gong[c], Xie Quan[b]

[a] State Key Laboratory of Pollution Control and Resource Reuse, School of the Environment, Nanjing University, Nanjing 210093, PR China
[b] School of Environmental and Biological Science and Technology, Dalian University of Technology, Dalian 116024, PR China
[c] Institute of Applied Ecology, Chinese Academy of Sciences, Wenhua Road 72, P.O. Box 417, Shenyang 110016, PR China

ARTICLE INFO

Article history:
Received 22 June 2009
Received in revised form
30 September 2009
Accepted 30 September 2009
Available online 6 October 2009

Keywords:
Photocatalytic activity
F–Si-codoped titania
ESR
Methyl orange

ABSTRACT

F–Si-co-modified TiO_2 (FST) samples with different ratios of fluorine to titanium (R_F) and silica to titanium (R_x), were successfully synthesized by ultrasound-assisted hydrolysis. The structure and properties of the as-prepared codoped titania were characterized by means of XRD, TEM, XPS, BET, UV–Vis diffuse reflectance spectra and ESR. XRD analysis showed that Si and F atoms prevented phase transition of anatase to rutile and suppressed the growth of titania crystalline. ESR results showed that the concentration of the active species (•OH) on 1%-FST$_{(R_x=10\%)}$ was higher than that on other FST samples and P25 titania. The improvement in photocatalytic activity relative to titania can be achieved by co-modifying fluorine and silica to fabricate FST composite material. The photocatalytic activity of FST powders for decomposition of methyl orange was affected by the content of fluorine and the content of silica. When the ratios of R_F and R_x were 1 and 10%, respectively, 1%-FST$_{(R_x=10\%)}$ shows the best among photocatalytic activity, which is much superior to P25 under UV–Vis irradiation. The possible reasons for the high photocatalytic activity of the FST powders were proposed in the paper. In addition, the stability of the FST powders in photocatalytic process was confirmed based on the XPS analysis.

1. Introduction

Semiconductor photocatalysis has been intensively investigated for its application to environmental pollutants' degradation [1–5]. The photocatalyst used is mainly focused on TiO_2 semiconductor due to its low cost, high stability and environmental friendly features. However, the photocatalytic activity of TiO_2 is not high enough for the requirements of practical applications. So improving its photocatalytic activity is still a principal challenge. The introduction of new active sites into TiO_2 should enhance the photocatalytic activity. Titania–silica mixed oxides [6–7] have aroused considerable interest for photocatalytic applications because of their high photocatalytic activity. This is partially explained by the intimate interaction of TiO_2 and SiO_2, which results in new structural and physicochemical properties such as quantum-sized crystallinity, high surface area, high adsorption capacity or high acidity [6–9].

Fluorinated TiO_2 has been often investigated in relation to doping ($TiO_{2-x}F_x$) [10–15] or surface complexation (F–TiO_2) [14–18]. It has been reported that fluoride doping improves the crystallinity of anatase and the photocatalytic reactivity [11–13]. In addition, $TiO_{2-x}F_x$ has fewer anion vacancies with a lower density of midgap states [10–12,15] and is more stable against photocorrosion. Surface fluorinated TiO_2 (F–TiO_2) has been investigated as a new surface modification method [19–21]. Some researchers have reported that the introduction of fluorine atoms into a photocatalytic system is effective for enhancing the photocatalytic activity of TiO_2. The higher photocatalytic oxidation in the F–TiO_2 suspension has been ascribed to the enhanced generation of mobile free •OH radicals, whereas most *•OH radicals generated from naked TiO_2 surface prefer to remain adsorbed [19]. In our previous work, silicon and fluorine atoms were simultaneously doped into the TiO_2 crystal lattice with the aims of introducing new active sites and enhancing the UV light absorption capacity of titania, a high reactive, photocatalyst F–Si-codoped titania (FST) is achieved. However, to our knowledge, there were no reports on the systematical synthesis of FST, except for our previous study on microwave-assisted photocatalytic degradation of PCP in the presence of FST, which was firstly prepared by ultrasound-assisted hydrolysis (UAH) [22].

In our previous work, we had successfully prepared F–Si-codoped titania (FST) photocatalyst that could work efficiently under UV–Vis irradiation. Herein, we further studied the effects of Si and F atoms on photocatalytic activity of titania samples to elucidate the reasons for exhibiting photocatalytic activity and to understand the role of doped F/Si atoms in UV–Vis photocatalysis. Moreover, the possible reasons on FST with high photocatalytic activity were discussed here.

* Corresponding authors. Tel.: +86 25 83593239; fax: +86 25 83593239.
E-mail address: yangdlut@126.com (S. Yang), envidean@nju.edu.cn (C. Sun).

0304-3894/$ – see front matter © 2009 Elsevier B.V. All rights reserved.
doi:10.1016/j.jhazmat.2009.09.158

2. Experimental and methods

2.1. Reagents and materials

5,5-dimethyl-1-pyrroline-*N*-oxide (DMPO) spin-trap reagent (Sigma Chemical Co.), tetraethylorthosilicate (TEOS), tetrabutylorthotitanate (TBOT), sulfuric acid, NH_4F and methyl orange were purchased from Shanghai Chemical Company, China, and all are of analytical purity grade.

2.2. Preparation of fluorine–silica-doped titania (FST) powders

Nanocrystalline titania powders were prepared by hydrolysis under ultrasonic irradiation [15]. TBOT and NH_4F were used as titanium and fluorine sources. TEOS was used as a precursor of the dopant. Mixture of TBOT (0.1125 mol) and TEOS was directly added dropwise to 900 mL NH_4F aqueous solution under vigorous stirring at room temperature. The atomic ratios of fluorine to titanium and silica to titanium hereafter were designated as R_F and R_x, respectively. When R_x was constant (10%), R_F were 0, 0.5, 1, 3, 10 and 20%, and R_F-F–Si-codoped titania was labeled as R_F-FST$_{(R_x=10\%)}$; R_F was constant (1%), R_x were 0, 5, 10 and 20%, and R_x-F–Si-codoped titania was labeled as 1%-FST$_{R_x}$. The formed FST samples were then radiated in an ultrasonic cleaning bath (KQ3200E, 40 kHz, 150 W) for 1 h, followed by aging in a closed beaker at room temperature for 24 h. After aging, these FST samples were dried at 100 °C for about 8 h in air in order to vaporize water in the gels and then grounded to fine powders to obtain dry gel, and finally calcined at different temperatures in air for 1 h.

2.3. Characterization

The crystal phase of FST samples was identified by X-ray diffraction with a X′TRA diffractometer made in ARL Company, Swiss. The average crystalline size of all samples can be estimated by the Scherrer formula: $L = 0.89\lambda/\beta\cos\theta$ (where L is the crystallite size, λ is the wavelength of the X-ray radiation (Cu Kα = 0.15418 nm), K is usually taken as 0.89, and β is the line width at half-maximum height, after subtraction of equipment broadening). The morphology of FST samples was characterized by transmission electron microscopy (TEM; Hitachi-600). Hitachi Company Measurement of BET surface area was performed using N_2 adsorption/desorption isotherms on a Micromeritics ASAP 2020. X-ray photoelectron spectroscopy (XPS) measurements were done on an ESC ALB MK-II XPS system with a monochromatic Al KR source and a charge neutralizer; all the binding energies were referenced to the C 1s peak at 285 eV of the surface adventitious carbon. ESR signals of radicals spin-trapped by DMPO were recorded on a Brucker ED-200D-SRC 10/12 spectrometer at ambient temperature under photoirradiation of a 180 W mercury lamp. The recorded spectra were taken into a personal computer with an image scanner and converted to a g value scale referring to a Mn^{2+} marker.

2.4. Photocatalytic experiment

The photocatalytic activity of FST powders for decomposition of methyl orange was investigated in a photocatalytic reactor shown in Fig. 1. A high-pressure mercury lamp (a 400 W high-pressure mercury lamp from Beijing light factory with a maximum wavelength of 365 nm, I_o = 1.50 mW cm^{-2}) was positioned vertically in a double-wall U-tube inside the cylindrical reactor surrounded by a circulating water tube to maintain reaction isothermally. The photocatalytic reactor has an effective volume of 150 mL. Additionally, the exterior wall of the reactor was covered with a reflecting aluminum. The reaction was performed under the following conditions: UV irradiation, vigorous stirring, and no airflow, 20 mg L^{-1} methyl orange and 0.18 g FST powder.

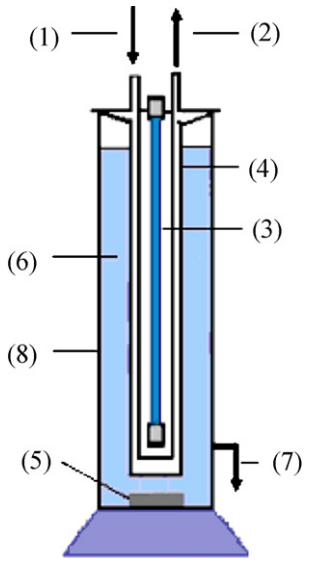

Fig. 1. Photoreactor system for methyl orange degradation. (1) Cooling water input, (2) water outflow, (3) UV lamp, (4) quartz sleeve, (5) stirrer bar, (6) reactant solution, (7) exhaust and (8) glass reactor

P25 titania particles (50 m^2/g) with crystalline structure of ca. 30% rutile and 70% anatase and primary particle size of ca. 21 nm were taken as a reference to test the photoactivity of the FST powders towards the degradation of methyl orange.

Concentration of methyl orange was determined using UV-1600 spectroscopy at wavelength λ = 480 nm quantitatively. Total organic carbon (TOC) was determined with Shimadzu TOC-5000 analyzer.

3. Results and discussions

3.1. Characterization of the FST powders

3.1.1. Crystal structure

The phase structure, crystallite size and crystallinity of titania play important roles in photocatalytic activity. XRD was used to investigate phase structure of the prepared R_F-FST$_{(R_x=10\%)}$ powders

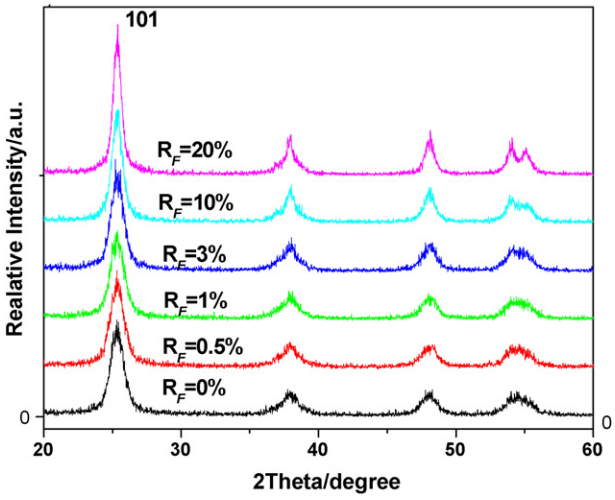

Fig. 2. XRD patterns of the R_F-FST$_{(R_x=10\%)}$ powders calcined at 550 °C for 1 h (R_F = 0, 0.5, 1%, 3%, 10% and 20%).

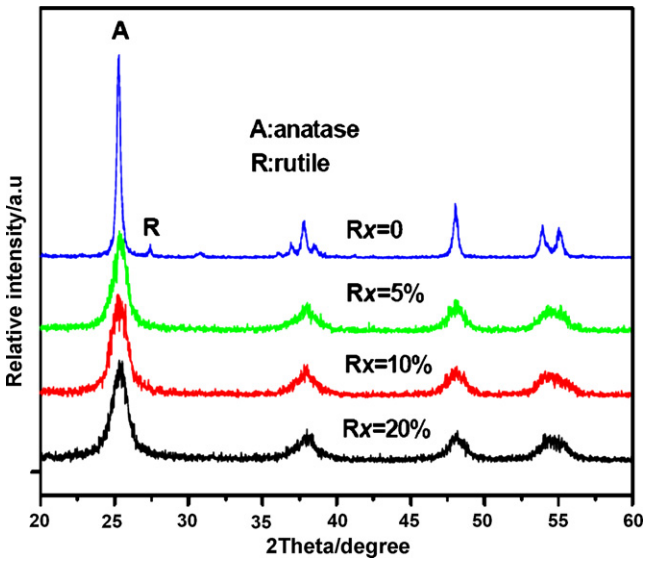

Fig. 3. XRD patterns of R_X-FST$_{(R_F=1\%)}$ powders calcined at 550 °C for 1 h (R_x = 0, 5, 10 and 20%).

after heat treatment at 550 °C for 1 h. Fig. 2 shows the effects of fluorine content on the phase structures of FST$_{(R_X=10\%)}$ powders calcined at 550 °C for 1 h. The major crystalline phase detected in all samples after doping fluorine is pure anatase. Apart from the diffraction peaks corresponding to anatase, there are no other diffraction peaks from $2\theta = 20°$ to 60° for all the R_F-FST$_{(R_X=10\%)}$ samples. It can be seen from the figure that the peak of anatase phase in all FST samples becomes much stronger and sharper with increasing fluorine content, indicating the higher crystallinity of anatase than that of pure titania. The average sizes of the samples with R_F = 0, 0.5, 1.0, 3.0, 10 and 20% were 4.9, 6.4, 7.1, 7.9, 8.5 and 9.3 nm, respectively.

Fig. 3 shows the influence of silica content on the phase structures of 1%-FST powders calcined at 550 °C 1 h. The major phase of the 1%-FST$_{R_X}$ powders with different R_X values was pure anatase. It is noteworthy that apart from the diffraction peaks corresponding to anatase, no other diffraction peaks could be observed from $2\theta = 20°$ to 60° for all of the R_X-FST$_{(R_F=1\%)}$ samples, indicating that silica exists in amorphous phase. It can be seen from the figure that the peak becomes broad with the increasing silica content, which indicates that the size of the samples become smaller [17]. The average sizes of the samples with R_X = 0, 5.0, 10 and 20% were 8.9, 7.4, 7.1 and 6.9 nm, respectively, which illustrates that the presence of silica can effectively inhibit the grain growth of catalyst. Furthermore, the crystallite size of the samples after silica modifying is smaller than that of the unmodified samples. It is thought that silica modifying prolongs the crystallization of anatase and retards the transformation of amorphous titania to anatase since the crystallinity of silica modified samples is lower than that of unmodified samples. Furthermore, the crystalline size of the samples after silicon and fluorine doping changed slightly, indicating that the silicon and fluorine did not alter the FST samples structure and remained the well anatase crystallization after the addition process.

Table 1
Effect of calcination temperature and R_F on BET surface area and pore parameters of R_F-FST$_{(R_X=10\%)}$ powders.

R_F (%)	Calcination temperature (°C)	BET (m^2/g)	Pore volume (mL g^{-1})	Pore size (nm)
1	100	346	0.433	2.2
0	550	196	0.279	5.8
0.5	550	185	0.273	6.0
1	550	178	0.268	6.4
3	550	170	0.263	7.8
5	550	162	0.259	9.6
10	550	139	0.254	11.2
20	550	124	0.248	12.6

Fig. 4 shows TEM photographs of 1%-FST$_{(R_X=10\%)}$ powders calcined at (a) 450 and (b) 550 °C for 1 h. It is obviously seen that the reactive temperature affects the morphologies of the sample. At 450 and 550 °C, some of the particles are fused together due to sintering, which explains the significant decrease in S_{BET} (shown in Table 1) with increasing calcination temperature.

3.1.2. XPS studies

The chemical states and concentrations of the Si/F atoms incorporated into the FST powders were investigated from the analysis of XPS spectra. The silicon and fluorine elements can be chemically adsorbed on the TiO_2 surface or doped into TiO_2 lattice, and the adsorbed elements can be removed by thermal treatment. The characterization was carried out after 773 K calcination for 1 h to eliminate the simply adsorbed F or Si species and to prove their doping. Fig. 5A shows the XPS spectrum of 3%-FST$_{(R_X=10\%)}$ powders prepared by ultrasound-assisted hydrolysis and calcination at 550 °C for 1 h. XPS peaks show that the 3%-FST$_{(R_X=10\%)}$ powders contain only Ti, O, Si and F elements and a trace amount of carbon.

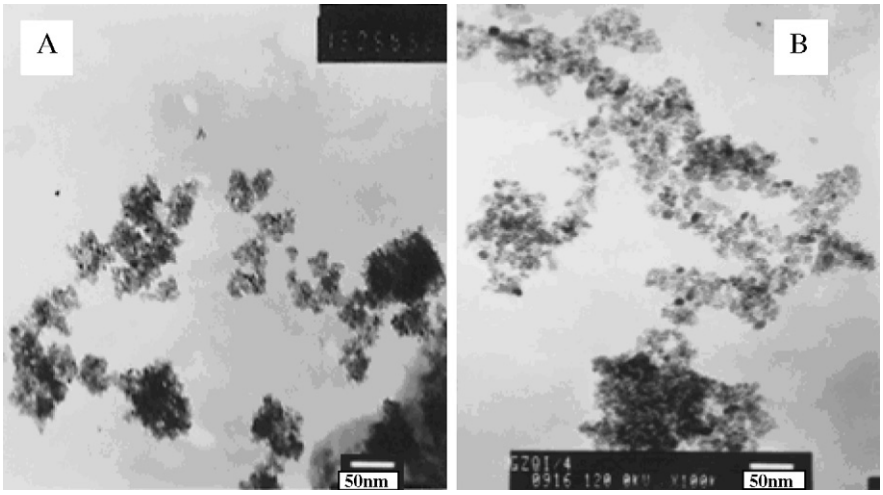

Fig. 4. TEM photographs of 1%-FST$_{(R_X=10\%)}$ powders prepared by ultrasonic-assisted hydrolysis calcination at 450 °C (A) and 550 °C for 1 h (B).

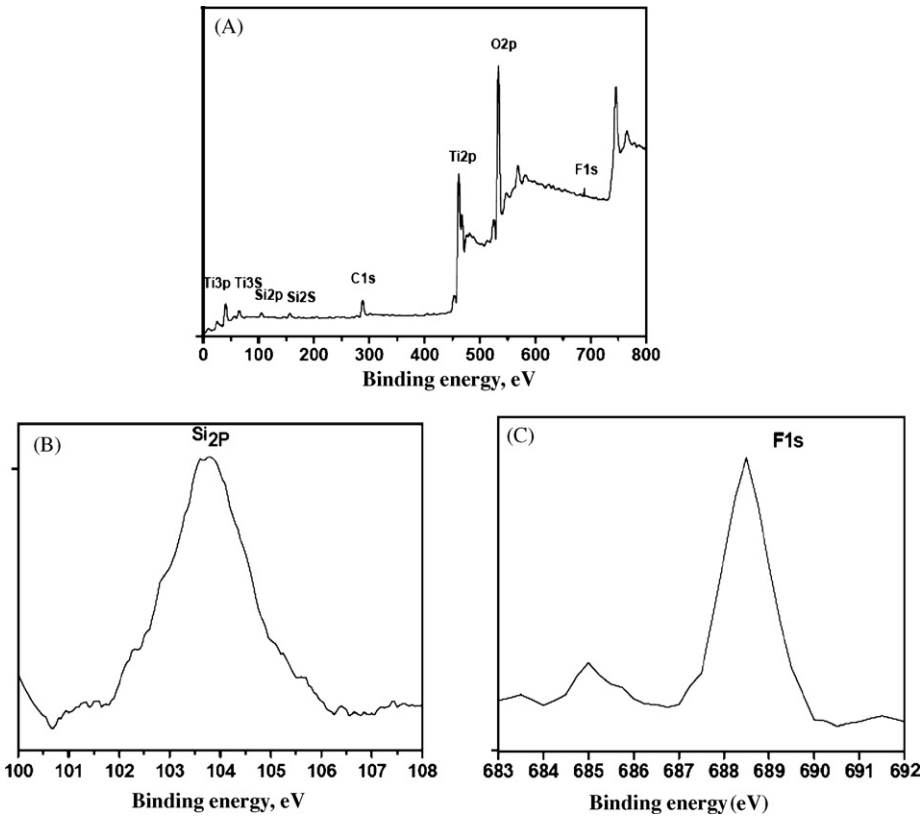

Fig. 5. XPS spectra of 3%-FST$_{(R_x=10\%)}$ powder (A) calcined at 550 °C for 1 h, Si 2p (B) and F 1s (C).

The following binding energies are used in our quantitative measurements: Ti 2p at 461 eV, O 1s at 533 eV, Si 2p at 103 eV, F 1s at 688 eV and C 1s at 285 eV. The atomic ratio of Ti:O:Si:F is about 1:2.13:0.13:0.011, which is basically close to the ratio of Ti/Si in the experiment [23]. The C element is ascribed to the residual carbon from precursor solution and the adventitious hydrocarbon from the XPS instrument itself. The XPS spectra of other samples are similar.

Fig. 5B and C shows the XPS spectra of the F 1s region and Si 2p, respectively, taken on the surface of the 3%-FST$_{(R_x=10\%)}$ sample calcinated at 550 °C for 1 h. The F 1s region is composed of two contributions. The main contribution is the F in solid solution $TiO_{2-x}F_x$, which is probably formed by nucleophilic substitution reaction of F^- ions and titanium alkoxide during the hydrolysis process [16,24,25] because of the fact that the ion radii of F^- and O^{2-} are similar. The minor contribution is assigned to F^- ions physically adsorbed on the surface of TiO_2. During the calcinations process, thermal energy can trigger the substitution of F^- for O^{2-} in the lattice of TiO_2. It is not too surprising that nonstoichiometric solid solutions of $TiO_{2-x}F_x$ are formed [26].

3.1.3. BET surface areas and pore structure

Since heterogeneous photocatalyst is affected by the surface area and pore structure, the effects of silicon and fluorine codoping on the BET surface area and the pore structure of FST samples were investigated here. Fig. 6 shows the pore size distribution curve calculated from the desorption branch of the nitrogen isotherm by the BJH method and the corresponding nitrogen adsorption–desorption isotherms (inset) of 1%-FST$_{(R_x=10\%)}$ powders calcined at 550 °C for 1 h. The sharp decline in desorption curve is indicative of mesoporosity, while the hysteresis between the two curves demonstrates that there is a diffusion bottleneck, possibly caused by nonuniform pore size. The pore size distribution calculated from the desorption branch of the nitrogen isotherm by the BJH (Barrett–Joyner–Halenda) method shows a narrow range of 5.0–10 nm with an average pore diameter of 7.5 nm.

Tables 1 and 2 show that all samples have mesoporous structures, which result from the pores formed between TiO_2 particles. These mesopores allow rapid diffusion of various reactants and products during photocatalytic reaction and enhance the rate of photocatalytic reaction. It can be noted from Table 1 that when $R_F = 1$, the FST$_{(R_x=10\%)}$ powders dried at 100 °C show a very large S_{BET} value of 346 m^2/g. However, all of the surface area, porosity and pore volume become smaller with increasing calcination temperature. The pore diameter increases due to the growth of titania

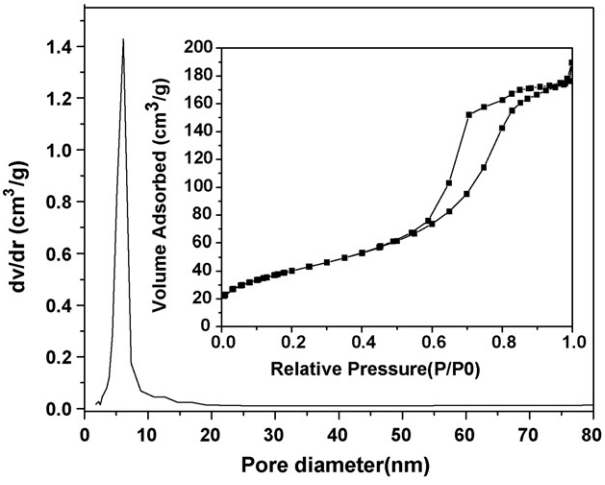

Fig. 6. Pore size distribution curve calculated from the desorption branch of the nitrogen isotherm by the BJH method and the corresponding nitrogen adsorption–desorption isotherms (inset) of 1%-FST$_{(R_x=10\%)}$ powders calcined at 550 °C for 1 h.

Table 2
Effect of R_x on BET surface area and pore parameters of R_x-FST$_{(R_F=1\%)}$ powder.

R_x (%)	Calcination temperature (°C)	BET (m^2/g)	Pore volume ($mL\,g^{-1}$)	Pore size (nm)
0	550	78	0.213	18.5
5	550	163	0.271	7.9
10	550	178	0.268	7.5
20	550	186	0.299	7.0

crystallites. Table 1 also shows that, at 550 °C, when $R_F = 0$, the S_{BET} value of FST$_{(R_x=10\%)}$ is higher than that of R_F-FST$_{(R_x=10\%)}$ ($R_F \neq 0$), which is possibly because the former has a smaller TiO_2 crystallite (6.4 nm). When R_x is constant 10%, with increasing R_F, the S_{BET} value of FST decreases steadily. This may be ascribed to the fact that the greater the amount of F^- ions in the TiO_2 xerogels, the stronger the promoting action of TiO_2 anatase crystallization. This would produce larger TiO_2 crystallites. Table 2 indicates that at 550 °C, when $R_F = 1$, with increasing R_x, the S_{BET} value of FST increases steadily. As we are all known, there is still argumentative one on whether activity of a photocatalyst is related to the catalyst surface area, but adsorption on the catalyst surface would at least help to "concentrate" the reactant molecules for the photoreactions and the photos might be scattered between the nano-sized titania particles [26]. Meanwhile, photogenerated electrons and vacancies as well as the adsorbed molecules might be able to diffuse more or less at the catalyst surface, causing the photoreactions to happen more easily [27]. The high specific surface area of pure titania and FST may help this process more efficiently in the photodegradation. Hence the series of FST catalysts show higher photoactivity than P25 in the decomposition of aqueous methyl orange solution.

3.1.4. UV–Vis spectra

As a photocatalyst, the wavelength distribution of the absorbed light is one of the important properties regardless of the quantum yield. The high photoactivity of FST samples can be attributed to the higher UV–Vis light absorbance, which can be easily proved by UV–Vis diffuse reflectance spectra. Fig. 7 shows the DRS spectra of prepared R_F-FST$_{(R_x=10\%)}$ powders with the different fluorine content. It is apparent that the absorption spectra of all samples show stronger absorption in the UV–visible range and a blue shift in the band gap absorption edge was observed, which may be explained in terms of the quantum size effects that emerge in semiconductors at small particle sizes. The band gap energy can be estimated from Kubelka–Munk function [25,28–29]. The calculated band gap

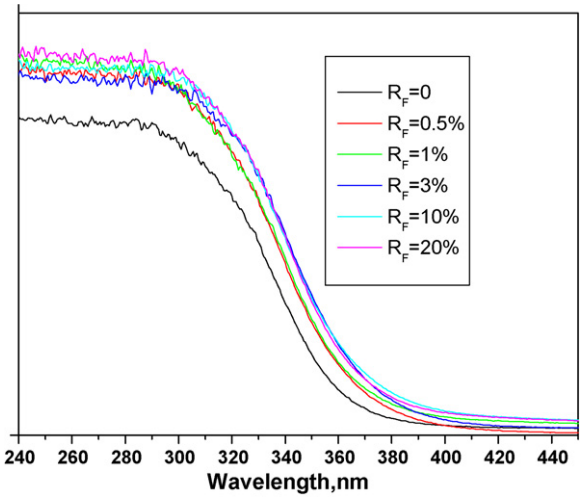

Fig. 7. UV–Vis spectra of R_F-FST$_{(R_x=10\%)}$ with different F/Ti ratios. $R_F = 0$, 0.5, 1, 3, 10 and 20%.

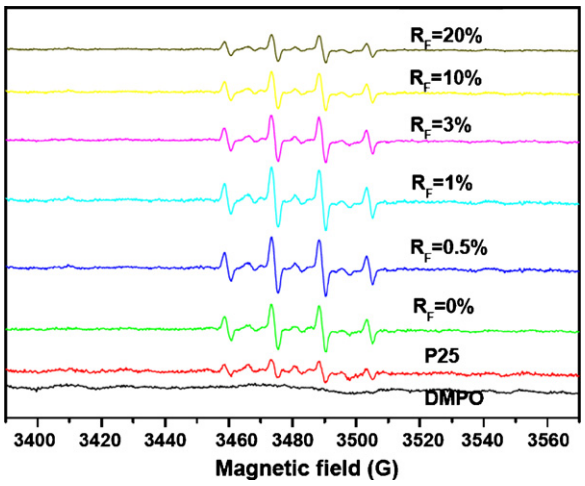

Fig. 8. DMPO spin-trapping ESR spectra under UV irradiation in R_F-FST$_{(R_x=10\%)}$ samples (calcined at 550 °C for 1 h) and P25 aqueous solutions ($R_F = 0$, 0.5, 1.0, 3.0, 10, 20%): catalyst loading, 0.5 g L^{-1}; DMPO concentration, 0.035 M.

energies of all FST samples with different R_F values (0, 0.5, 1, 3, 10 and 20%) are about 3.31, 3.28, 3.26, 3.24, 3.22 and 3.21 eV, respectively.

3.2. ESR signal analysis of DMPO-•OH

DMPO traps hydroxyl and superoxide radicals with the formation of nitrone spin adducts, which are more stable and can be detected by ESR spectroscopy [21]. The ESR spin-trap technique (with DMPO) was employed to probe the nature of the reactive oxygen species generated from R_F-FST$_{(R_x=10\%)}$ calcined 550 °C for 1 h under UV irradiation ($R_F = 0$, 0.5, 1, 3, 10, 20%). Fig. 8 illustrates the electron paramagnetic resonance spectra of R_F-FST$_{(R_x=10\%)}$-DMPO, P25-DMPO and DMPO alone systems. There are the characteristic four peaks of DMPO-•OH with intensity 1:2:2:1 in the ESR signal, which are similar to the results reported by others for the •OH adduct [21,30]. Furthermore, the peak intensity of •OH generated from 1%-FST$_{(R_x=10\%)}$ was greatly higher than that from other R_F-FST$_{(R_x=10\%)}$ samples and P25, which indicated the photocatalytic activity of 1%-FST$_{(R_x=10\%)}$ is the best among all samples. It is obvious that the content of fluorine affects the photocatalytic activity of R_F-FST$_{(R_x=10\%)}$ photocatalyst, there is an optimum content, namely 1%, as shown in Fig. 8. The ESR signals for the spin adducts DMPO-OOH• and/or DMPO-O_2• should also have been detected. However, these latter two spin adducts were not observed in this study. It is well documented that the superoxide radical anions are produced first and remain stable in an organic solvent medium (at least in methanol) [23], while the superoxide radical anions are unstable in H_2O system, for example, $O_2^{\bullet -}$ readily converted to H_2O_2 and O_2. Another possible reason is the slow reactions between •OOH/$O_2^{\bullet -}$ and DMPO, which are several orders of magnitude lower than formation of the DMPO-•OH spin adduct [24]. In addition, the transition from DMPO-OOH• and DMPO-O_2• to DMPO-•OH was too fast [24].

3.3. Photocatalytic degradation of methyl orange

Experiments were conducted under three different conditions: (i) in the dark in the presence of 1%-FST$_{(R_x=10\%)}$ calcined 550 °C for 1 h, (ii) only UV irradiation without photocatalyst, (iii) under UV irradiation in the presence of pure titania calcined 550 °C for 1 h and (IV) under UV irradiation in the presence of 1%-FST$_{(R_x=10\%)}$ calcined at 550 °C for 1 h. In addition, the variation of TOC value with irradiation time was carried out in 1%-FST$_{(R_x=10\%)}$ aqueous suspen-

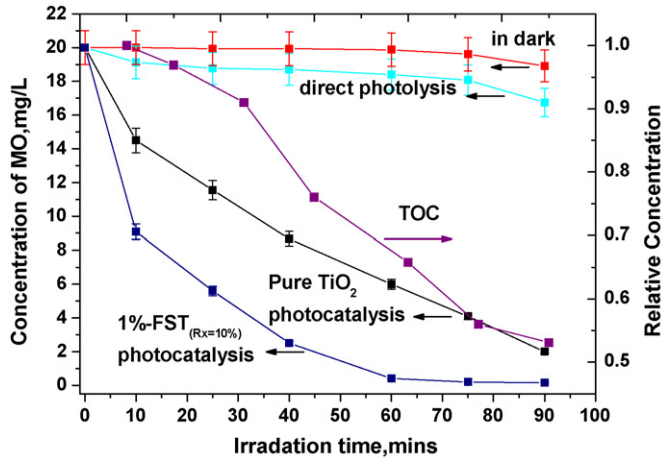

Fig. 9. Methyl orange concentration and TOC vs. reaction time in different processes. Photocatalyst: 1%-FST$_{(R_x=10\%)}$ calcined at 550 °C for 1 h.

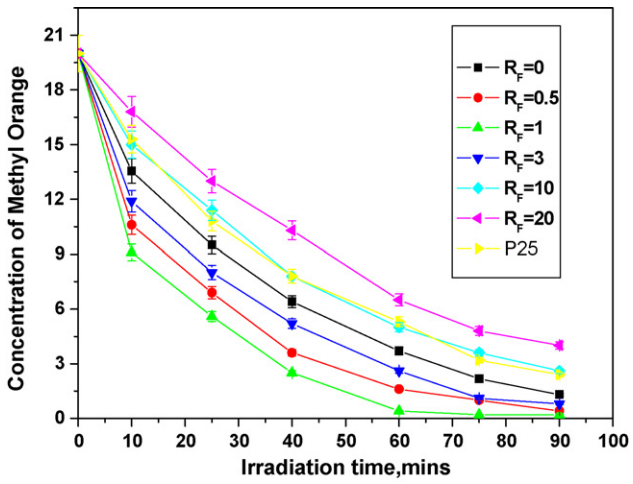

Fig. 10. Methyl orange concentration vs. UV irradiation time with R_F-FST$_{(R_x=10\%)}$ photocatalysts calcined at 550 °C for 1. R_F = 0, 0.5, 1.0, 3.0, 10, 20% and Degussa P25.

sion. The results are illustrated in Fig. 9, where the concentration of methyl orange is plotted again the reaction time.

A little decrease in methyl orange occurred in the dark treatment, i.e., 0.9% of the initial substrate disappeared after 1 h of continuous stirring. This phenomenon might be due to the adsorption of photocatalyst FST-1%. In direct photolysis without photocatalyst, about 8% degradation efficiency was observed for 1 h irradiation; and 16.3% for 1.5 h. When methyl orange with 1%-FST$_{(R_x=10\%)}$ powders in aqueous dispersion was exposed to UV light, the concentration of methyl orange decreased markedly. About 87.5–99% of methyl orange was degraded within 40–60 min of the reaction. It was clearly observed from Fig. 9 that the TOC value in aqueous solution decreased gradually with the irradiation time and the removal of 48% TOC was observed in 90 min. However, when methyl orange with pure titania powders in aqueous dispersion was exposed to UV light, removal efficiency of methyl orange was 90% in 90 min. The photocatalytic degradation followed pseudo-first-order kinetics, the kinetic constant for pure titania and 1%-FST$_{(R_x=10\%)}$ catalysts is 0.0228 and 0.0587 min^{-1}, respectively. It indicated that 1%-FST$_{(R_x=10\%)}$ was a photocatalyst with high photocatalytic activity and can be utilized for water purification.

3.3.1. Effect of fluorine content

The photocatalytic activity of FST samples is sensitive to the content of fluorine and the content of silica, and then their effects are discussed subsequently. It is significant to investigate the dependence of photocatalytic activity of the R_F-FST$_{(R_x=10\%)}$ on the doped fluorine content. The photocatalytic degradation followed pseudo-first-order kinetics. Results are presented in Fig. 10 and Table 3. The photocatalytic degradation rate of methyl orange firstly increased with an increase of fluorine content in the catalyst in the range of 0–1%, which might be due to the increase of the crystallinity [11,13,21,31]. However, higher fluorine content (>1%) did not favor the further enhancement of the photoactivity of R_F-FST$_{(R_x=10\%)}$, since the specific surface area (shown in Fig. 7 and Table 1) decreased in spite of the better crystallinity of anatase and SiO_2 did not exhibit photocatalytic activity. The maximum degradation rate occurred on 1%-FST$_{(R_x=10\%)}$ and it was about 2.5 times higher than that of P25, an excellent photocatalyst recognized [1,25]. It should be noted that the photocatalytic activity of 1%-FST$_{(R_x=10\%)}$ is the best among all the R_F-FST$_{(R_x=10\%)}$ samples in this study (shown in Fig. 9). The difference in surface area, UV adsorption and more hydroxyl radical was responsible for this discrepancy. The increasing surface area shown in Fig. 6 and Table 1 was facilitating the adsorption of reactants and enhancing the speed of photocatalytic reaction. The increasing intensive absorbance shown in Fig. 7 resulted in the increase in rate of transfer of photogenerated electrons to the surface, leading to effective participation in the surface reaction [32]. The increasing hydroxyl radical presented in Fig. 8 resulted in faster degradation of methyl orange in aqueous solutions. From the above result, it could be concluded that the increase of surface area, absorption in UV region and hydroxyl radical are the prominent factors for high photocatalytic activity of methyl orange decomposition and the optimum ratio of fluorine to titania is 1%. Moreover, another reason on enhancement of FST powders was that ultrasonic irradiation enhanced hydrolysis of titanium, silicon alkoxide and NH_4F, crystallization of the gel and the enhancement of dispersion of FST (shown in Fig. 4).

Table 3
The kinetic constants and regression coefficients of methyl orange photocatalysis on R_F-FST$_{(R_x=10\%)}$ calcined at 550 °C for 1 h.

Photocatalyst	Kinetic constant (min^{-1})	R^2	Ratio of K to K_{P25}
R_F = 0	0.0296 ($K1$)	0.9955	1.25
R_F = 0.5%	0.0414 ($K2$)	0.9898	1.75
R_F = 1%	0.0587 ($K3$)	0.9881	2.48
R_F = 3%	0.0365 ($K4$)	0.9846	1.54
R_F = 10%	0.0231 ($K5$)	0.9981	0.98
R_F = 20%	0.0185 ($K6$)	0.9943	0.78
Degussa P25	0.0236 (K_{P25})	0.9964	1.00

3.3.2. Effect of silica content

The photocatalytic activity of the prepared R_x-FST$_{(R_F=1\%)}$ powder for the decomposition of methyl orange was affected by the doped silica content. The results were presented in Fig. 11 and Table 4. The photocatalytic degradation rate of methyl orange firstly increased with an increase in the silica content in range of 0–10% due to decrease in average sizes as is shown in the XRD analysis in Fig. 3 and Table 2 and the increase in surface hydroxyl radicals presented in Fig. 8. However, higher fluorine content (over 10%) did not favor

Table 4
The kinetic constants and regression coefficients of methyl orange photocatalysis on R_x-FST$_{(R_F=1\%)}$ calcined at 550 °C for 1 h.

Photocatalyst	Kinetic constant (min^{-1})	R^2	Ratio of K to K_{P25}
R_x = 0	0.0287 ($K7$)	0.9881	1.21
R_x = 5%	0.0380 ($K8$)	0.9758	1.61
R_x = 10%	0.0587 ($K3$)	0.9881	2.48
R_x = 20%	0.0293 ($K9$)	0.9889	1.24

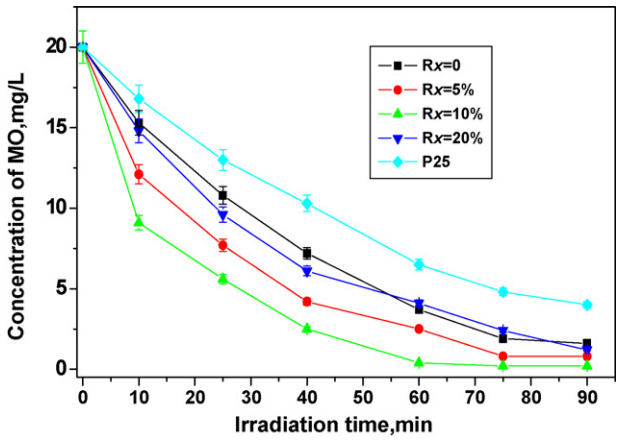

Fig. 11. Methyl orange concentration vs. UV irradiation time with R_x-FST$_{(R_F=10\%)}$ photocatalysts calcined at 550 °C for 1. R_x = 0, 5, 10, 20% and Degussa P25.

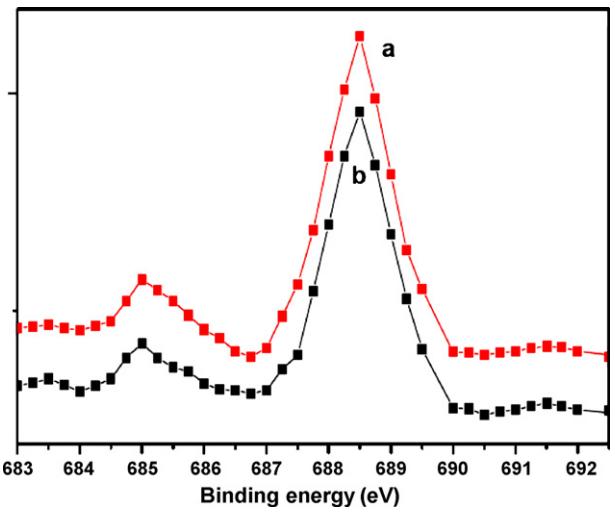

Fig. 12. XPS spectra of 1%-FST$_{(R_x=10\%)}$ powders calcined at 550 °C for 1 h (a) before use, (b) after 10 times use.

further enhancement of the photoactivity of FST because the crystallinity of anatase decreased in spite of the larger specific surface area (Table 2) and silica did not exhibit photocatalytic activity.

The efficiency of the photocatalytic degradation over 1%-FST$_{(R_x=10\%)}$ has been also analyzed using the quantum yield. The quantum yield of a reaction is defined as the number of MO molecules being decomposed (degraded) per photon absorbed (Eq. (1)).

$$\phi = \frac{\text{Number of molecules decomposed}}{\text{Number of photons of light absorbed}} \quad (1)$$

The photodegradation rate constant k of MO under the monochromatic light source can also be used for the calculation of its reaction quantum yield using Eq. (2).

$$\phi = \frac{k}{2.303 I_{0,\lambda} \varepsilon_{D,\lambda} l} \quad (2)$$

ϕ is the reaction of quantum yield (dimensionless), $I_{0,\lambda}$ is the intensity of the incident light at 365 nm (1.38×10^{-6} Einstein L^{-1} S^{-1}), $\varepsilon_{D,\lambda}$ is the molar absorptivity of MO at 365 nm (2.36×10^{-4} cm^{-1} M^{-1}), l is the path length of reaction tube which is 24 cm for the irradiated solution.

The quantum yields of the photodegradation of MO with 1%-FST$_{(R_x=10\%)}$ and TiO_2-P25 were determined to be 0.55 and 0.22, respectively. About 2.5 times enhancement in photocatalytic degradation of MO with 1%-FST$_{(R_x=10\%)}$ is observed under these conditions.

3.4. Possible reasons for the high photocatalytic activity of the FST powders

The FST powder demonstrated high photocatalytic activity for degradation of methyl orange under UV irradiation. The reasons can be closely related to the doped Si and F atoms.

Firstly, the doped Si atoms in FST improved the photocatalytic oxidation of methyl orange in aqueous solutions, partially due to the decreasing of catalyst particle and the increasing high surface area [8,9]. Another possible reason was the presence of high surface acidity on FST powders. The cation of dopant oxide entered the lattice of its host oxide and retained its original coordination number and a charge imbalance was created. It has been found that the new acidic sites created by lattice substitution had Bronsted acid character instead of Lewis acid character in the silica–titania system [33]. Kwon et al. and Li et al. confirmed that the enhancement in surface acidity improved the activity of a photocatalytic system [34,35]. Moreover, the surface acidic site also acts as an electron acceptor [36,37], which enhances the separation of photogenerated electrons and holes, i.e., to increase k value, and improve the photocatalytic activity.

Secondly, the beneficial effects produced by doped F atoms in FST powders on the photocatalytic activity might be as follows: (1) F-doping led to the improvement of anatase crystallinity, which result in increasing of photocatalytic activity [11,13]. (2) F-doping improved UV adsorption of catalysts. The rate of the photocatalytic reaction is proportional to $(I_\alpha \phi)^n$ ($n = 1$ for low light intensity and $n = 1/2$ for high light intensity), where I_α is the number of photons absorbed by photocatalyst per second and ϕ is the efficiency of the band gap transition. Therefore, an increase in α (absorption coefficient) or $I_\alpha \phi$ and a decrease in k_{rec} (rate constant of recombination of the charge carriers) would increase the rate at which the photogenerated electrons reach the surface, leading to effective participation in the surface reaction. The absorption coefficient α can be calculated from the measured absorbance (A) using the following equation [38,39],

$$\alpha = \frac{2.303 \rho \times 10^3}{lcM} A \quad (3)$$

where the density $\rho = 3.9\ g\ cm^{-3}$, molecular weight $M = 79.9\ g\ mol^{-1}$, c is the molar concentration of FST, and l is the optical path length, respectively. On the basis of UV adsorption spectra in Fig. 7, it is obviously observed that the intensity of absorption below 400 nm increases with increasing fluorine content due to the increase in band gap transition in FST samples. The enhancement of the photocatalytic activity with F-doping can be partly explained in terms of an increase in $I_\alpha \phi$ resulting from intensive absorbance in the UV regions. Therefore, the enhancement of the photocatalytic activity with FST comes from intensive absorbance in the UV regions. (3) F-doping resulted in the enhanced mobile free •OH radicals whereas most OH radicals generated on naked TiO_2 surface preferred to remain adsorbed [19]. Therefore, the photogenerated electron in the FST powders could easily diffuse from the inner region to the surface of the particles to take part in the surface photochemical reaction [40,41].

Consequently, introduction of fluorine and silica can increase the specific surface area, UV adsorption, active radicals and the transfer rate of photogenerated electrons to the surface of photocatalysts and then promote photocatalytic activities of FST catalyst.

3.5. Stability of FST powders

Both the hydrofluoric acid and fluoride ion are severe poison. So we have to understand whether there are any possibilities that the FST is decomposed releasing hydrofluoric acid or fluoride ion in the water system when FST as a photocatalyst was used in water purification. From the XPS analysis of F 1s (shown in Fig. 12), there is no noticeable change in the XPS of F 1s on the 3%-FST$_{(R_x=10\%)}$ powders after 10 times of photocatalytic reaction for 90 min. The results also indicated that the degradation efficiencies were rather stable with the relative standard deviation of 3.5%. It is considered that the observed chemical stability of the FST powders led to the stable catalytic activities.

Therefore, the introduction of fluorine and silicon to titania is beneficial for degradation of the target contaminant and it is possible for FST powders to be used as photocatalysts in water purification.

4. Conclusion

F–Si-co-modified TiO_2 nanoparticles with pure anatase phases were prepared by ultrasonic hydrolysis method. The specific surface area and crystallinity of anatase titania were improved by Si modifying. Moreover, Si and F atoms prevented phase transition of anatase to rutile and suppressed the growth of titania crystalline. The FST samples showed stronger absorption in the UV–visible region and ESR signals indicated that the concentration of the active species ($^{\bullet}$OH) on 1%-FST$_{(R_x=10\%)}$ was higher than that on other FST samples.

The photocatalytic activity of FST powders was obviously affected by the content of doped silica and fluorine. The photocatalytic activity of FST firstly increased with an increase of fluorine content in the catalyst in the range of 0–1%, higher fluorine content (>1%) did not favor the further enhancement of the photoactivity of R_F-FST$_{(R_x=10\%)}$, and there is an optimum content of silica in the catalyst. The highest photocatalytic activity of 1%-FST$_{(R_x=10\%)}$ was observed and its degradation rate is 2.48 times that of P25. This may be ascribed to a synergetic effect of its unique surface characteristics, doped Si atoms, and doped F atoms. The stability of the FST powders in photocatalytic process was confirmed based on the XPS analysis. The experiment results indicate that the FST powder is a very interesting and promising photocatalytic material and has good potential for application to water purification.

Acknowledgments

This work was supported by National Natural Science Foundation of China (20707009), National Major Project of Science & Technology Ministry of China (Grant no. 2008ZX07421-002 and 2008ZX08526-003) and Opening Foundation for Key Laboratory of Industrial Ecology and Environmental Engineering (no. 0703) for financial support.

References

[1] M.R. Hoffmann, S.T. Martin, W. Choi, D.W. Bahnemann, Environmental applications of semiconductor photocatalysis, Chem. Rev. 95 (1995) 69–96.
[2] X.Z. Li, H.S. Liu, Development of an E-H_2O_2/TiO_2 photoelectrocatalytic oxidation system for water and wastewater treatment, Environ. Sci. Technol. 39 (12) (2005) 4614–4620.
[3] S. Cho, W. Choi, Solid-phase photocatalytic degradation of PVC–TiO_2 polymer composites, J. Photochem. Photobiol. A 143 (2001) 221–228.
[4] X. Quan, S. Yang, X. Ruan, H. Zhao, Preparation of titania nanotubes and their environmental applications as electrode, Environ. Sci. Technol. 39 (2005) 3770–3775.
[5] E. Bae, W. Choi, Highly enhanced photoreductive degradation of perchlorinated compounds on dye-sensitized metal/TiO_2 under visible light, Environ. Sci. Technol. 37 (2003) 147–152.
[6] N. Husing, B. Launay, D. Doshi, G. Kickelbick, Mesostructured silica-titania mixed oxide thin films, Chem. Mater. 14 (2002) 2429–2432.
[7] V. Lafond, P.H. Mutin, A. Vioux, Control of the texture of titania–silica mixed oxides prepared by nonhydrolytic sol–gel, Chem. Mater. 16 (2004) 5380–5386.
[8] R. Mariscal, M. Lopez-Granados, J.L.G.F. ierro, J.L. Sotelo, C. Martos, R. Van Grieken, Morphology and surface properties of titania-silica hydrophobic xerogels, Langmuir 16 (2000) 9460–9467.
[9] D.C.M. Dutoit, U. Gobel, M. Schneider, A. Baiker, Titania–silica mixed oxides. I. Influence of sol–gel and drying conditions on structural properties, J. Catal. 153 (1995) 165–176.
[10] S.N. Subbarao, Y.H. Yun, R. Kershaw, K. Dwight, A. Wold, Electrical and optical properties of the system $TiO_{2-x}F_x$, Inorg. Chem. 18 (1979) 488–492.
[11] A. Hattori, M. Yamamoto, H. Tada, S. Ito, A promoting effect of NH_4F addition on the photocatalytic activity of sol–gel TiO_2 films, Chem. Lett. 8 (1998) 707–708.
[12] A. Hattori, M. Yamamoto, H. Tada, S. Ito, Photoreactivity of sol–gel TiO_2 films formed on soda-lime glass substrates: effect of SiO_2 underlayer containing fluorine, Langmuir 15 (1999) 5422–5425.
[13] J.C. Yu, J. Yu, W. Ho, Z. Jiang, L. Zhang, Effects of F-doping on the photocatalytic activity and microstructures of nanocrystalline TiO_2 powders, Chem. Mater. 14 (2002) 3808–3816.
[14] C.M. Wang, T.E. Mallouk, Photoelectrochemistry and interfacial energetics of titanium dioxide photoelectrodes in fluoride-containing solutions, J. Phys. Chem. 94 (1) (1990) 423–428.
[15] C.M. Wang, T.E. Mallouk, Wide-range tuning of the titanium dioxide flat-band potential by adsorption of fluoride and hydrofluoric acid, J. Phys. Chem. 94 (10) (1990) 4276–4280.
[16] C. Minero, G. Mariella, V. Maurino, D. Vione, E. Pelizzetti, Photocatalytic transformation of organic compounds in the presence of inorganic ions. 2. Competitive reactions of phenol and alcohols on a titanium dioxide–fluoride system, Langmuir 16 (6) (2000) 8964–8972.
[17] M.S. Vohra, S. Kim, W. Choi, Effects of surface fluorination of TiO_2 on the photocatalytic degradation of tetramethylammonium, J. Photochem. Photobiol. A 160 (2003) 55–60.
[18] M. Lewandowski, D.F. Ollis, Halide acid pretreatments of photocatalysts for oxidation of aromatic air contaminants: rate enhancement, rate inhibition, and a thermodynamic rationale, J. Catal. 217 (2003) 38–46.
[19] C. Minero, G. Mariella, V. Maurino, E. Pelizzetti, Photocatalytic transformation of organic compounds in the presence of inorganic anions. 1. Hydroxyl-mediated and direct electron-transfer reactions of phenol on a titanium dioxide–fluoride system, Langmuir 16 (2000) 2632–2641.
[20] D.W. Lee, S.K. Ihm, K.H. Lee, Mesostructure control using a titania-coated silica nanosphere framework with extremely high thermal stability, Chem. Mater. 17 (2005) 446–4467.
[21] E. Finkelstein, G.M. Rosen, E.J. Rauckman, Spin trapping of superoxide and hydroxyl radical: practical aspects, Arch. Biochem. Biophys. 200 (1980) 1–16.
[22] S.G. Yang, H.B. Fu, C. Sun, Z.Q. Gao, Rapid photocatalytic destruction of pentachlorophenol in F–Si-comodified TiO_2 suspensions under microwave irradiation, J. Hazard. Mater. 161 (2009) 1281–1287.
[23] N. Ma, X. Quan, Y.B. Zhang, S. Chen, H.M. Zhao, Integration of separation and photocatalysis using an inorganic membrane modified with Si-doped TiO_2 for water purification, J. Membr. Sci. 335 (2009) 58–67.
[24] J. Zhao, T. Wu, K. Wu, K. Oikawa, H. Hidaka, N. Serpone, Photoassisted degradation of dye pollutants. 3. Degradation of the cationic dye rhodamine B in aqueous anionic surfactant/TiO_2 dispersions under visible light irradiation: evidence for the need of substrate adsorption on TiO_2 particles, Environ. Sci. Technol. 32 (1998) 2394–2400.
[25] X. Dong, J. Tao, Y.Y. Li, H. Zhu, Enhanced photoelectrochemical properties of F-containing TiO_2 sphere thin film induced by its novel hierarchical structure, Appl. Surf. Sci. 255 (2009) 7183–7187.
[26] A. Piscopo, D. Robert, J.V. Weber, Comparison between the reactivity of commercial and synthetic TiO_2 photocatalysts, J. Photochem. Photobiol. A: Chem. 139 (2001) 253–256.
[27] J.X. Li, J.H. Xu, W.L. Dai, K.N. Fan, One-pot synthesis of twist-like helix tungsten-nitrogen-codoped titania photocatalysts with highly improved visible light activity in the abatement of phenol, Appl. Catal. B 82 (2008) 233–243.
[28] Y. Wang, B. Wu, Q. Xu, Preparation and characterization of nanosized anatase TiO_2 cuboids for photocatalysis, Appl. Catal. B 59 (2005) 139–146.
[29] Q.H. Zhang, L. Gao, J.K. Guo, Effects of calcination on the photocatalytic properties of nanosized TiO_2 powders prepared by $TiCl_4$ hydrolysis, Appl. Catal. B 26 (2000) 207–215.
[30] T. Yamaki, T. Umebayashi, T. Sumita, S. Yamamoto, M. Maekawa, A. Kawasuso, H. Itoh, Fluorine-doping in titanium dioxide by ion implantation technique, Nucl. Instrum. Method Phys. Res. B 306 (2003) 254–258.
[31] H. Kominami, S. Murakami, M. Kohno, Y. Kera, K. Okada, B. Ohtani, Stoichiometric decomposition of water by titanium(IV) oxide photocatalyst synthesized in organic media: effect of synthesis and irradiation conditions on photocatalytic activity, Phys. Chem. Chem. Phys. 3 (2001) 4102–4106.
[32] H. Hidaka, J. Zhao, E. Pelizzetti, N. Serpone, Photodegradation of surfactants. 8. Comparison of photocatalytic processes between anionic DBS and cationic BDDAC on the titania surface, J. Phys. Chem. 96 (1992) 2226–2232.
[33] J.C. Yu, J. Yu, L. Zhang, W. Ho, Enhancing effects of water content and ultrasonic irradiation on the photocatalytic activity of nano-sized TiO_2 powders, J. Photochem. Photobiol. A 148 (2002) 263–271.
[34] X. Fu, L.A. Clark, Q. Yang, M.A. Anderson, Enhanced photocatalytic performance of titania-based binary metal oxides: TiO_2/SiO_2 and TiO_2/ZrO_2, Environ. Sci. Technol. 30 (1996) 647–653.
[35] Y.T. Kwon, K.Y. Song, W.I. Lee, G.J. Chio, Y.R. Do, Photocatalytic behavior of WO_3-loaded TiO_2 in an oxidation reaction, J. Catal. 191 (2000) 192–199.

[36] D. Li, H. Haneda, S. Hishita, N. Ohashi, Visible-light-driven N-F-codoped TiO_2 photocatalysts. 2. Optical characterization, photocatalysis, and potential application to air purification, Chem. Mater. 17 (10) (2005) 2596–2602.
[37] D. Li, H. Haneda, Morphologies of zinc oxide particles and their effects on photocatalysis, Chemosphere 51 (2003) 129–137.
[38] A.V. Emeline, G.N. Kuzmin, D. Purevdorj, V.K. Ryabchuk, N.J.S. Serpone, Spectral dependencies of the quantum yield of photochemical processes on the surface of wide band gap solids. 3. Gas/solid systems, J. Phys. Chem. B 103 (2000) 1325–1331.
[39] S.G. Yang, Y.Z. Liu, C. Sun, Preparation of anatase TiO_2/Ti nanotube-like electrode and its high photoelectrocatalytic activity for the degradation of PCP in aqueous solution, Appl. Catal. A-Gen. 301 (2006) 284–291.
[40] D. Li, H. Haneda, Photocatalysis of sprayed nitrogen-containing Fe_2O_3–ZnO and WO_3–ZnO composite powders in gas-phase acetaldehyde decomposition, J. Photochem. Photobiol. A 160 (2003) 203–212.
[41] S.G. Yang, X. Quan, X.Y. Li, Y.Z. Liu, S. Chen, G.H. Chen, Preparation, characterization and photoelectrocatalytic properties of nanocrystalline Fe_2O_3/TiO_2, ZnO/TiO_2, and $Fe_2O_3/ZnO/TiO_2$ composite film electrodes towards pentachlorophenol degradation, Phys. Chem. Chem. Phys. 6 (2004) 654–659.